Journal of Materials Science: Materials in Electronics (2018) 29:7952–7956
https://doi.org/10.1007/s10854-018-8797-6

Effect of additional Zn^{2+} dopant on the ferromagnetic properties of Co-doped CeO_2 nanoparticles prepared by sol–gel method

Shenghong Yang[1] · Zhijie Jiang[1] · Yueli Zhang[2]

Received: 3 November 2017 / Accepted: 20 February 2018 / Published online: 23 February 2018

Abstract
Effect of additional Zn^{2+} dopant on the ferromagnetism (FM) of Co doped CeO_2 nanoparticles was studied. The Zn and Co co-doped CeO_2 nanoparticles ($Ce_{0.97-x}Zn_xCo_{0.03}O_2$: where $x = 0$, 0.01, 0.03, 0.05) were prepared by sol–gel technique. The crystal structure, morphology, and magnetic properties were analyzed by X-ray diffraction (XRD), scanning electron microscopy (SEM), Raman spectroscopy (Raman) and physical property measurement system (PPMS). XRD and Raman studied showed that certain amount of Zn^{2+} can readily be incorporated into the lattice of Co doped CeO_2 with single-phase of CeO_2 original cubic fluorite crystal structure, and no ferromagnetic secondary phase was observed. SEM images show Zn and Co co-doped CeO_2 nanoparticles were spherical and uniform size. The PPMS studied indicate that the room-temperature FM of Co doped CeO_2 nanoparticles increase with additional Zn^{2+} dopant. This result is helpful in understanding the origin of FM in diluted magnetic oxides (DMO) as well as improving the magnetic property of DMO.

1 Introduction

Physical properties and potential applications of semiconductor nanomaterials have been studied intensively [1–3]. Diluted magnetic semiconductors (DMS) have attracted the attention of the scientific community because of their potential for combining semiconductor and magnetic properties that are possible to use electronic charge and spin at the same time in a material. Room temperature ferromagnetism (FM) of the DMS by transition metal doped oxide semiconductor or insulator (TM-DMO) is the focus of today's research. The TM-DMO material combines the spin and charge of carriers, thus the implementation of spintronic devices is possible by using TM-DMO materials [4]. The discovery of more suitable doped elements and the development of various TM-DMO materials are the main tasks of the present [5–7]. The origin of room temperature FM in TM-DMO materials is another focus of the investigation. The reports in the literature are different, some even contrary, but it is generally believed that the ferromagnetic exchange in TM-DMO is mainly due to defects, electron transfer and oxygen vacancy (Vo) [7–9]. Among many oxides, rare earth oxide of cerium oxide (CeO_2) has attracted special attention. CeO_2 is widely used in luminescence, polishing, UV absorption, automobile exhaust purification, solid oxide fuel cells, optical coatings and oxygen sensors. In addition, CeO_2 is a typical wide band gap oxide semiconductor. The structure of CeO_2 belongs to cubic fluorite type, with lattice constant matching well with Si. Therefore, it is considered as a potential replacement for Si semiconductor. Recent studies have found room temperature FM in undoped CeO_2 and doped CeO_2 samples. These findings stimulate interest in the study of CeO_2 systems [8–10]. This is because the Ce ions in CeO_2 based diluted magnetic oxides (DMO) can have a variety of ionic states (+2, +3, and +4), Therefore, defects in CeO_2 based DMO are easy to manipulate. This is convenient to verify the mechanism of FM induced by defects. Second, the cubic structure of CeO_2 can accommodate a large number of oxygen vacancies, thus Vo in CeO_2 based DMO can be controlled. It is easy to verify the ferromagnetic coupling mechanism based on Vo by experiment. Third, CeO_2 based DMO are easy to integrate with semiconductor materials, this makes preparation of dilute magnetic/semiconductor superlattice structures easy. Therefore, new type of spin functional device can be developed. For understanding the origin of room temperature FM, a systematic study on doped CeO2 is demanded.

✉ Shenghong Yang
stsyshh@mail.sysu.edu.cn

[1] School of Physics, Sun Yat-sen University, Guangzhou 510275, China

[2] School of Materials and Engineering, Sun Yat-sen University, Guangzhou 510275, China

In the present work, Zn^{2+} was chosen as additional dopants for Co doped CeO_2 DMO systems. The Zn and Co co-doped CeO_2 nanoparticles ($Ce_{0.97-x}Zn_xCo_{0.03}O_2$: where $x = 0, 0.01, 0.03, 0.05$) were synthesized by sol–gel technique. The crystal structure, morphology, and magnetic properties were analyzed by X-ray diffraction (XRD), scanning electron microscopy (SEM), Raman spectroscopy and physical property measurement system (PPMS). Effect of additional Zn^{2+} dopant on the FM of Co doped CeO_2 nanoparticles has been discussed.

2 Experiments

Preparation of Zn and Co co-doped CeO_2 samples ($Ce_{0.97-x}Zn_xCo_{0.03}O_2$: where $x = 0, 0.01, 0.03, 0.05$) was done by sol–gel technique. The precursor solutions were prepared as follows. Stoichiometric amount of Ce(III) nitrate hexahydrate ($Ce(NO_3)_3{\cdot}6H_2O$), cobaltous nitrate ($Co(NO_3)_2{\cdot}6H_2O$) and zinc acetate dihydrate ($Zn(CH_3COO)_2{\cdot}2H_2O$) was used to obtain desired compositions. These solutes were completely dissolved in 2-methoxyethanol with stirring for 1 h at 65 °C, and then 3 h at room temperature. Acetylacetone ($CH_3COCH_2COCH_3$) was added to the solution as a stabilizer. According to previous reported results [5, 7–12], the optimal FM was obtained from Co-doped CeO_2 DMO system with the nominal Co content of 3 at.%. So here we kept Co doping concentration as a constant of 3 at.% with the variation of Zn^{2+} doping content from 0 to 5 at.%. Zn doping was achieved by the introduction of appropriate amount of $Zn(CH_3COO)_2{\cdot}2H_2O$. These precursor solutions were put in a furnace for 24 h at 100 °C to eliminate excess water and form the xerogel. Then, the xerogel was calcined at 700 °C for 2 h to eliminate organic materials and form a powder.

The crystal structure of $Ce_{0.97-x}Zn_xCo_{0.03}O_2$ powders were characterized by using RIGAKU D-MAX 2200 VPC X-ray diffractometer (XRD) equipped with a Cu-Kα ($\lambda = 1.54$ Å) source. The Raman spectroscopy of these powders was analyzed by a Confocal Micro-Raman Spectrometer (inVia Reflex, Renishaw) with 514 nm excitation source under air ambient condition. The morphology of the samples was observed by a thermal field SEM (Quanta 400F, FEI/OXFORD/HKL). Energy dispersive spectroscopy (EDS) was used to determine the amount of doping in the powder. Magnetic properties were investigated by a commercial physical property measurement system (PPMS, QUANTUM DESIGN, MOOEL 6000). In Table 1, some properties of $Ce_{0.97-x}Zn_xCo_{0.03}O_2$ powders, such as Zn content determined by EDS (x_{EDS}), particle size (D), saturation moment (M_s), and coercivity (H_C) are shown.

Table 1 Some properties of $Ce_{0.97-x}Zn_xCo_{0.03}O_2$ powders: Zn content determined by EDS (x_{EDS}), particle size (D), saturation moment (M_s), and coercivity (H_C)

Zn content x	x_{EDS}	D (nm)	M_s (emu/g)	H_C (Oe)
0.00	0.00	16.7	0.0018	305.28
0.01	0.009	14.6	0.0022	480.03
0.03	0.032	14.2	0.0031	508.83
0.05	0.054	11.9	0.0040	567.62

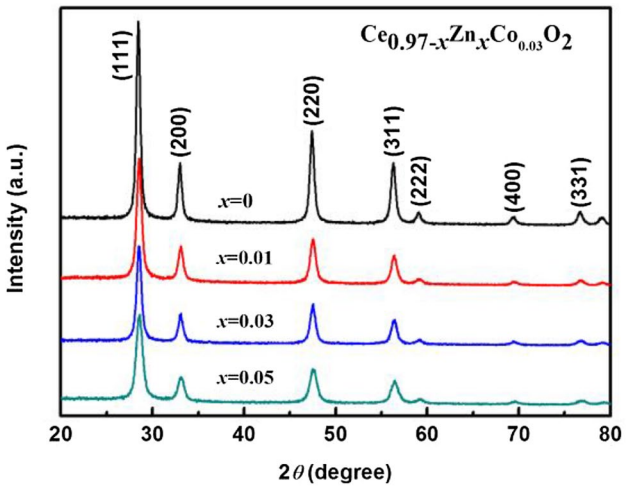

Fig. 1 The XRD patterns of the $Ce_{0.97-x}Zn_xCo_{0.03}O_2$ powders

3 Results and discussion

The XRD patterns of the $Ce_{0.97-x}Zn_xCo_{0.03}O_2$ (where $x = 0, 0.01, 0.03, 0.05$) powders are depicted in Fig. 1. The obtained XRD patterns matched the powder diffraction data for CeO_2 obtained using JCPDF 34-0394, which suggests a cubic symmetry belonging to the *Fm-3m* space group. Within the XRD detection limit, no extra diffraction peak related to the second phases of Co or Zn, which confirms the complete solubility of Zn and Co ions in the ceria crystal structure. This indicates that Zn and Co substituted for Ce in CeO_2 host without changing the fluorite crystal structure. From Fig. 1, it is seen that all diffraction peaks were broadened, which indicated the fine nature of the small particles. By using Debye Scherrer formalism $D = 0.89\lambda/\beta\cos\theta$, where β is the full-width at half-maximum in radians, θ is the Bragg's angle in degrees, and λ is the wavelength of X-rays (1.54 Å for Cu-Kα), the average particle size of $Ce_{0.97-x}Zn_xCo_{0.03}O_2$ powders has been determined from the peak (111) broadening in the XRD patterns. The calculated particle size was 16.7, 14.6, 14.2 and 11.9 nm for x values of 0, 0.01, 0.03, and

0.05, respectively. The particle size and the peak intensity decrease with the increase of the amount of Zn^{2+} (see Table 1).

Figure 2 shows the SEM images of $Ce_{0.97-x}Zn_xCo_{0.03}O_2$ powders with $x = 0$, 0.03. The particles were spherical, uniform size, and good dispersion. The particle size was about 20 nm for $Ce_{0.97-x}Zn_xCo_{0.03}O_2$ powders with $x = 0$, 0.03, which agree well with the results calculated from Scherrer equation. The EDS spectrum (data not shown), which was collected from different parts of the samples, indicted that the $Ce_{0.97-x}Zn_xCo_{0.03}O_2$ powders consist of Ce, Co, Zn and O only. A semi-quantitative analysis confirmed that the Co and Zn content in the samples were consistent with the design of our experiments (see Table 1).

The structure of the $Ce_{0.97-x}Zn_xCo_{0.03}O_2$ nanoparticles was further studied by Raman spectroscopy. Figure 3 shows the Raman spectrum of the $Ce_{0.97-x}Zn_xCo_{0.03}O_2$ (where $x = 0$, 0.01, 0.03, 0.05) nanoparticles, measured in the 200–700 cm^{-1} range. A strong band at 462.5 cm^{-1} was observed for all nanoparticles. This band belongs to the lattice mode (F_{2g}) of the cubic fluorite metal dioxides. It related to a first-order symmetrical stretching mode of the Ce–O_8 vibrational unit. This band (462.5 cm^{-1}) is sensitive to any disorder in the oxygen sublattice [13]. The F_{2g} mode shifts to the lower frequencies with additional Zn^{2+} dopant. This shift indicates the increase in the tensile stress of the crystal lattice caused by defects, such as vacancies generated when Co and Zn substitutes for Ce in the CeO_2 matrix [14]. A weak band at 545 cm^{-1} was also observed for Zn and Co co-doped CeO_2 nanoparticles. This band is attributed to the oxygen hole absorption peak [15], which indicates Vo was generated due to charge compensation in the Zn and Co co-doped CeO_2 nanoparticles. The

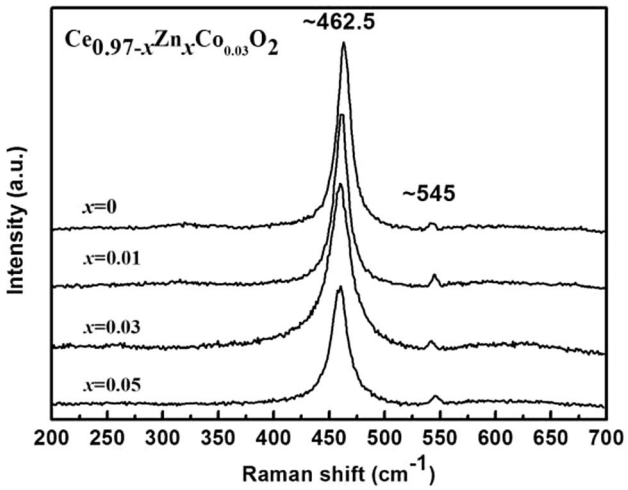

Fig. 3 Raman spectra of the $Ce_{0.97-x}Zn_xCo_{0.03}O_2$ nanoparticles

peak intensity of the Raman modes was found to decrease by increasing the Zn doping concentrations. We think that the increased Zn concentrations lead to shrinkage in unit cell volume. This increases the optical absorption. Thus the intensity of the Raman peaks decreases. Therefore, the observed decrease in the intensity of Raman active mode is the result of additional Zn doping induced structural modification in Co-doping CeO_2 nanoparticles. Furthermore, we have not observed any Raman active modes of Zn- or Co-related oxide in this study. Hence, the Raman studies strengthened the XRD data and help us to conclude that: (i) all the samples are in nanocrystalline form; (ii) the Vo maybe present in the samples, and Vo concentration is varied with additional Zn doping; and (iii) no secondary

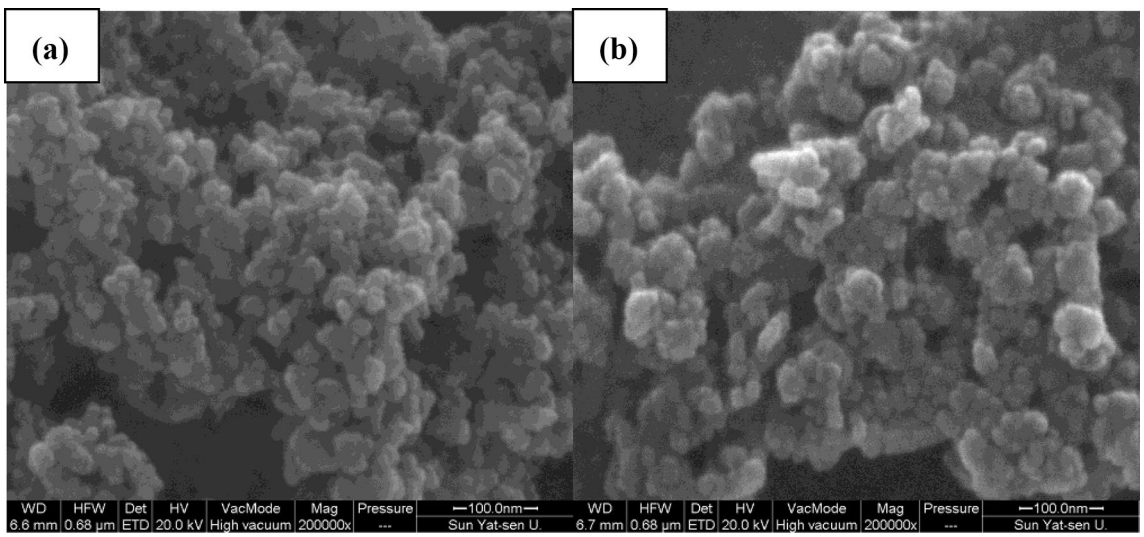

Fig. 2 The SEM images of $Ce_{0.97-x}Zn_xCo_{0.03}O_2$ powders with $x = 0$ (**a**) and $x = 0.03$ (**b**)

phases could be detected, indicative of substitutional doping of Zn and Co.

Magnetic properties of the $Ce_{0.97-x}Zn_xCo_{0.03}O_2$ (where $x=0$, 0.01, 0.03, 0.05) nanoparticles were studied by using the commercial physical property measurement system (PPMS, QUANTUM DESIGN, MOOEL 6000). Figure 4 dislpays magnetization (M) versus field (H) curves of $Ce_{0.97-x}Zn_xCo_{0.03}O_2$ nanoparticles measured at 300 K. It can be seen from the M (H) curves that $Ce_{0.97-x}Zn_xCo_{0.03}O_2$ nanoparticles show the magnetic hysteresis loop, which gives the indication of ferromagnetic ordering at 300 K. The coercive field (H_C) values calculated from hysteresis loops were in the range from 300 to 550 Oe for different Zn^{2+} concentration (shown in the Table 1). The saturation magnetization (M_s) for $x=0$, 0.01, 0.03, and 0.05 are 0.0018, 0.0022, 0.0031, and 0.004 emu/g, respectively. It is found that the M_s increases as the additional Zn^{2+} dopant content increases (see Table 1).

Combining with the analysis of XRD and Raman spectra, it could be concluded that the room temperature FM observed in the $Ce_{0.97-x}Zn_xCo_{0.03}O_2$ nanoparticles may be intrinsic because it is very easy to rule out any impurity for the magnetic signal in $Ce_{0.97-x}Zn_xCo_{0.03}O_2$ nanoparticles. Effect of additional Zn^{2+} dopant on the room temperature FM of Co doped CeO_2 nanoparticles possibly results from Vo or defects. In fact, the Vo appear to increase with increases in the Zn^{2+} content according to the Raman investigation before. The enhancement of room temperature FM in $Ce_{0.97-x}Zn_xCo_{0.03}O_2$ nanoparticles could be attributed to interactions between the Zn^{2+} and uncompensated acceptor defects that are incorporated inside the CeO_2 crystal lattice during the calcination of the samples. As well known that, Zn^{2+} substitution of Ce^{4+} will produce more Vo due to charge compensation, and the formation of V_O increases with the increase of the amount of Zn^{2+}. The formation of

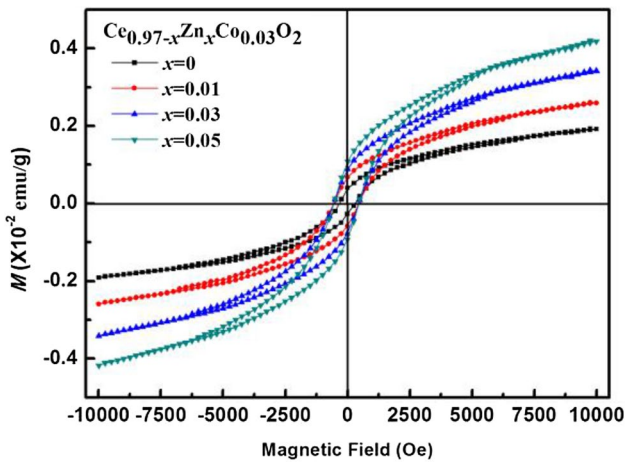

Fig. 4 M (H) measurements at 300 K of the $Ce_{0.97-x}Zn_xCo_{0.03}O_2$ nanoparticles

V_O is confirmed by our Raman spectra before. On the basis of F-center mediated ferromagnetic coupling mechanism used in insulated DMO [16–19], more Vo will provide more coupling centers thus induce larger M_s. The increase in Zn doping concentration favored ferromagnetic interactions because most of the V_O are formed. Therefore, the M_s is enhanced with additional Zn^{2+} dopant. Defects have also been reported as one of the possible reason for the FM origination [20]. Owing to the quite close ionic radius, doped Zn^{2+} would preferably substitute the crystal Ce^{4+} rather than locate at interstice. The substitution of Ce^{4+} by Zn^{2+} will also produce the lattice distortion or form some other defects, because the ionic radius of Zn^{2+} (0.09 nm) is smaller than that of Ce^{4+} (0.097 nm). Basing on the FM mechanism of the defects/V_O through the F-center exchange interaction, it is readily to expect the M_s enhancement by additional Zn^{2+} dopant.

4 Conclusions

In summary, the Zn and Co co-doped CeO_2 nanoparticles ($Ce_{0.97-x}Zn_xCo_{0.03}O_2$: where $x=0$, 0.01, 0.03, 0.05) were synthesized by sol–gel technique. The XRD and Raman results indicated that all the samples had a face-centered cubic structure and that no secondary phase was detected. The influence of additional Zn^{2+} dopant on the FM of Co-doped CeO_2 nanoparticles was studied. Results indicate that the FM of Co-doped CeO_2 nanoparticles was enhanced with additional Zn^{2+} dopant. The FM behavior can be attributed to the presence of dopant ions mediated by Vo. We conclude that Zn^{2+} is a good candidate to be incorporated into the lattice of CeO_2 with the substitution of Ce^{4+}, which would enhance the FM of Co-doped CeO_2 nanoparticles.

Acknowledgements This work was supported by the National Natural Science Foundation of China under Grant Nos. 61176010 and 61172027.

References

1. A. Sobhani-Nasab, A. Ziarati, M. Rahimi-Nasrabadi et al., Res. Chem. Intermed. **43**(11), 6155–6165 (2017)
2. A. Ziarati, A. Sobhani-Nasab, M. Rahimi-Nasrabadi et al., J. Rare Earths **35**(4), 374–381 (2017)
3. A. Sobhani-Nasab, Z. Zahraei, M. Akbari et al., J. Mol. Struct. **1139**, 430–435 (2017)
4. T. Diet, H. Ohno, F. Matsukura et al., Science **287**, 1019–1022 (2000)
5. R.K. Singhal, P. Kumari et al., J. Phys. D: Appl. Phys. **44**, 165002 (2011)
6. N. Doğan, A. Bingölbali, L. Arda, J. Magn. Magn. Mater. **373**, 226–230 (2015)
7. Y.Q. Song, H.W. Zhang et al., J. Appl. Phys. **102**, 043912 (2007)

8. A. Tiwari, V.M. Bhosle, S. Ramachandran et al., Appl. Phys. Lett. **88**, 142511 (2006)
9. B. Vodungbo, Y. Zheng, F. Vidal et al., Appl. Phys. Lett. **90**(1–3), 062510 (2007)
10. V. Femandes, J.J. Klein, N. Mattoso et al., Phys. Rev. B **75**, 121304 (2007)
11. E.M. Waleed, A.A. Al-Ghamdia, F.A. Al-Agelc et al., Mater. Res. Bull. **72**, 154–159 (2015)
12. P. Sumalin, P. Supree, M. Santi, J. Appl. Phys. **112**, 113904 (2012)
13. J.R. Mcbride, K.C. Hass, B.D. Poindexter, W.H. Weber, J. Appl. Phys. **76**, 2435–2441 (1994)
14. B. Choudhury, A. Choudhury, Curr. Appl. Phys. **13**, 217–223 (2013)
15. M.S. Anwar, S. Kumar, F. Ahmed, N. Arshi, G.S. Kil, D.W. Park et al., Mater. Lett. **65**, 3098–3101 (2011)
16. M. Venkatesan, C.B. Fitzgerald. J.M.D. Coey, Nature **430**, 630–630 (2004)
17. J.M.D. Coey, A.P. Douvalis, C.B. Fitzgerald et al., Appl. Phys. Lett. **84**, 1332–1334 (2004)
18. F. Meng, C. Zhang, Q.H. Bo et al., Mater. Lett. **99**, 5–7 (2013)
19. Y. Jiang, J.B. Adams, M. van Schilfgaarde, J. Chem. Phys. **123**, 064701 (2005)
20. W. Lee, S.Y. Chen, Y.S. Chen, C.L. Dong, H.J. Lin, C.T. Chen, A. Gloter, J. Phys. Chem. C **118**, 26359–26367 (2014)